Design and characterization of broadband acoustic composite metamaterials

Bogdan-Ioan Popa* and Steven A. Cummer†
Department of Electrical and Computer Engineering, Duke University, Durham, North Carolina 27708, USA
(Received 29 August 2009; revised manuscript received 27 October 2009; published 25 November 2009)

We demonstrate a method to design nonresonant acoustic composite metamaterials made of periodic arrangements of highly subwavelength unit cells composed of one or more inclusions embedded in a fluid. The inclusion geometry determines the degree of anisotropy and effective material parameters, and its nonresonant nature makes it suitable for large bandwidth applications. To characterize the resulting acoustic metamaterial, two sets of normal incidence plane wave reflection and transmission simulations on thin samples are performed. Applying this method, we show that samples as thin as one unit cell in the propagation direction are sufficient to characterize the composite. Different simple unit cell geometries were considered in order to bound the achievable material parameters of such composites. The large range of obtainable parameters, including strong anisotropy, makes this approach suitable for creating the materials needed for applications of transformation acoustics. As an example, we illustrate our method by designing and simulating a physically realizable implementation of a beam-bending flat lens that theoretically requires complex inhomogeneous materials not easily available in nature.

DOI: 10.1103/PhysRevB.80.174303 PACS number(s): 46.40.Cd, 41.20.Jb

I. INTRODUCTION

Exotic acoustic device concepts, such as the acoustic scattering reducing coatings, i.e., "cloaks of silence,"[1–5] lead recently to increased interest in the development of engineered acoustic composite metamaterials that can expand the range of responses to acoustic excitation available in natural materials. Negative bulk and Poisson modulii, as well as negative mass densities, have been shown to exist in resonant composites.[6–9] Their resonant behavior, however, implies a narrow frequency band of operation, which limits the applications of such composites.

In many applications, however, negative effective parameters are not required and broadband solutions are possible. For example, alternating layers of very thin materials[4,10] have been shown to approximate the inhomogeneous and anisotropic profiles required to obtain the above mentioned acoustic cloaking shell. Perforating the thin shells to create arrays of thin plates[11] also can yield the needed anisotropic effective mass density with a structure that is potentially simpler to fabricate. The generality of transformation acoustics,[2,12] through which coordinate transformations on acoustic fields can be realized with suitably designed complex acoustic materials, creates the possibility of many interesting applications if the hierarchical electromagnetic metamaterial design approach, from unit cells to arrays of cells,[13,19] can be replicated for acoustic metamaterials.

Here, we build on this past work to extend a proven simulation-based design approach for electromagnetic metamaterials[13] to nonresonant acoustic metamaterials. Our acoustic metamaterial is assumed to be made of subwavelength unit cells containing one or more inclusions. There is an extensive literature on the homogenization of such composite acoustic materials (see, for example, Refs. 14–18 for a short list). Our aim here is to demonstrate a numerical approach capable of handling arbitrarily complex composites for obtaining the nonlocal effective properties that describe how a wave interacts with and propagates through such a material. Section II demonstrates the approach with a simple example, while Sec. III shows that the effective parameters extracted with our approach can be used to design a composite that interacts with an incident wave essentially exactly how a prescribed continuous material would.

For simplicity, we illustrate our method in a two-dimensional space, however, our analysis can be extended with identical conclusions to three-dimensional structures.

II. DESIGN AND CHARACTERIZATION OF COMPOSITE METAMATERIALS

Consider an inviscid fluid having zero shear modulus. An acoustic wave propagating inside such a medium is governed by the conservation of momentum and mass equations, which, for small perturbations, can be written [we assume an $\exp(j\omega t)$ time dependence]

$$\nabla p + j\omega\bar{\bar{\rho}}(\mathbf{r})\rho_0\mathbf{v} = 0$$

$$j\omega p + B(\mathbf{r})B_0\nabla\cdot\mathbf{v} = 0, \tag{1}$$

where p is the pressure, $\mathbf{v}$ is the fluid velocity, B is the bulk modulus relative to B_0, and $\bar{\bar{\rho}}$ is the generalized density tensor[16] whose components are relative to ρ_0. For illustration purposes, we assume that B_0 and ρ_0 are the parameters of air, i.e., $B_0=141$ kPa and $\rho_0=1.29$ kg/m^3.

We consider composite media that have the general structure presented in Fig. 1(a). They are made of periodic arrays of unit cells, each cell composed of one or more inclusions positioned inside a background fluid. It is common to treat these media as homogeneous materials characterized by effective material parameters, B_{eff} and $\bar{\bar{\rho}}_{\text{eff}}$, as long as the unit cell dimensions are highly subwavelength. We assume, without loss of generality, that the mass density tensor[16] has zero off-diagonal terms, since any tensor can be diagonalized by a suitable rotation of the coordinate system. Our analysis is done in a two-dimensional space with inclusions whose sym-

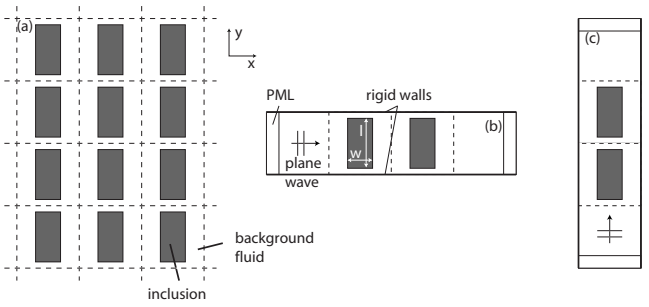

FIG. 1. Simulation setup used to analyze a bulk composite medium. (a) The composite medium is made of array of unit cells that contain one or more inclusions; (b) simulation setup used to retrieve the effective material parameters B_{eff} and ρ^x_{eff}. Rigid walls are used to simulate infinite medium in the transverse direction. The simulation domain is terminated with reflectionless perfect matched layers (PMLs); (c) simulation setup used to obtain the effective material parameters B_{eff} and ρ^y_{eff}.

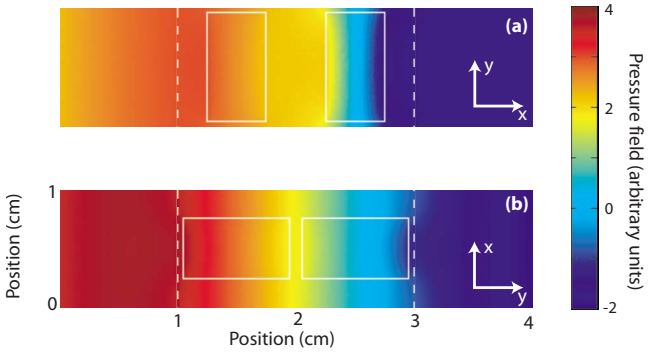

FIG. 2. (Color online) Pressure field of a wave propagating at a frequency for which the background fluid wavelength is an order of magnitude bigger than the unit cell dimension (i.e., $\lambda_{\text{bk}}=10$ cm). Notice that the fields are almost invariable in the transverse direction. (a) Fields used to recover B_{eff} and ρ^x_{eff}; (b) fields used to recover B_{eff} and ρ^y_{eff}.

metry axes are aligned with the coordinate directions. Consequently, two components of the density tensor, ρ^x_{eff} and ρ^y_{eff}, are needed to specify our materials.

Such composites can be analyzed theoretically, for example, in the quasistatic approximation using relations similar to the Clausius-Mosotti equation for electromagnetic mixed media.[20] However, the effective acoustic material parameters can be obtained in numerical simulations, without any approximations, using a method adapted from electromagnetics[13,21] and based on the fact that the wave equations and boundary conditions are similar for acoustics and electromagnetics, as pointed out in Ref. 1. The details of this method applied in the acoustics case can be found in Ref. 22. More specifically, acoustic plane waves are sent normally incident on a composite slab of finite thickness in the propagation direction and infinite extent in the transverse direction, and the reflection and transmission coefficients are recorded. These coefficients are inverted in order to obtain the effective modulus, B_{eff}, and the component of the density tensor in the direction of propagation. Since, in our case, the density tensor contains two nonzero components, we need two sets of measurements to determine both of them.

Figure 1(b) shows the simulation domain used to numerically retrieve B_{eff} and ρ^x_{eff}. As the composite under test is made of arrays of unit cells, its thickness can only be an integer multiple of the unit cell dimension. For simplicity the cell is a square having edge a, and contains one rectangular piece of steel of length l and width w. The background fluid is assumed to be air. The parameters of steel relative to those of air are $B=8\times10^5$ and $\rho=6131$. Notice that our inclusions are solids in which pressure waves are usually described by elastodynamic equations more complex than Eq. (1). However, these inclusions are much smaller than the wavelength, they do not fill the whole section of the unit cell, and there is a large contrast between their material parameters and those of air, so that the overall behavior of the composite is that of a fluid and not of a solid.

For illustration purposes, the medium pictured in Fig. 1(b) contains two cells in the propagation direction, however, we will show shortly that samples as thin as one cell are enough in order to characterize a bulk medium. We chose $a=1$ cm, $l=0.9a$, and $w=0.5a$. In order to simulate infinite extent in the direction perpendicular to the propagation direction, rigid walls are used on the top and bottom of the simulation domain. Perfectly matched layers border the left and right boundaries. A pressure plane wave propagating in the x direction from left to right is normally incident on the sample, and the reflected and transmitted waves are computed using the commercial package COMSOL Multiphysics. Figure 2(a) shows the computed pressure fields inside and around the sample. These fields are used to calculate the reflection and transmission coefficients relative to the sample boundaries, which in turn are needed to calculate B_{eff} and ρ^x_{eff}.[22]

A similar procedure is used to retrieve the other density component, ρ^y_{eff}: this time, the incident plane wave propagates in the y direction through a thin sample of the bulk composite, as depicted in Fig. 1(c). As before, the sample is two unit cells in the propagation direction and has infinite extent in the transverse direction. The pressure fields computed in this case are presented in Fig. 2(b).

Figure 3 shows the retrieved effective material parameters for both these simulations as a function of wavelength inside the background fluid, λ_{bk}, expressed as a multiple of the unit cell diameter. The retrieved material parameters are generally constant with the wavelength, as expected. Thus, we obtain almost constant effective material parameters over a large band of frequencies, from 0 Hz to roughly $v_{\text{bk}}/(10a)=3430$ Hz, where $v_{\text{bk}}=343$ m/s is the speed of sound in the background fluid (i.e., air). The practical implication of this observation is that we can increase the bandwidth of the composite metamaterial simply by scaling down the geometry of the unit cell. This contrasts with the behavior of resonant metamaterials, for which geometry scalings do not affect their bandwidth, but controls their narrowband working frequency.

For wavelengths comparable to the unit cell diameter, the homogenization theory that allows to associate effective material parameters to the composite material loses its effectiveness and the medium starts to behave more like a sonic crystal[23] than a homogeneous material. As a consequence,

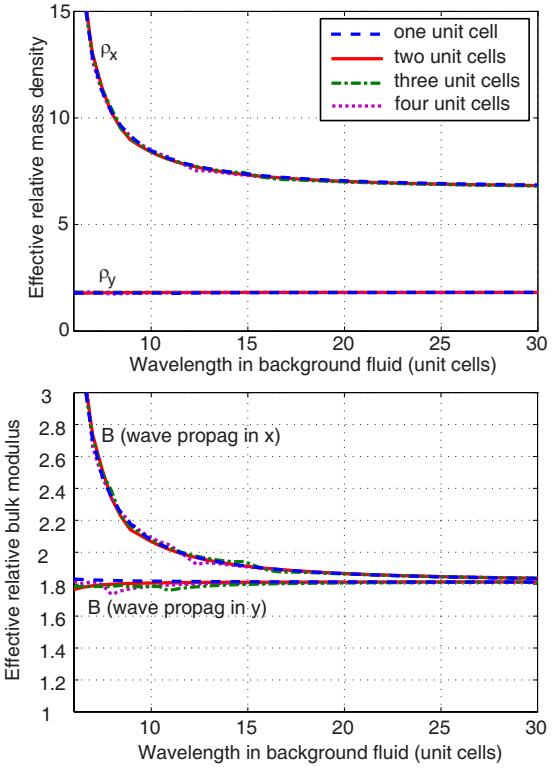

FIG. 3. (Color online) Effective material parameters (top: mass density; bottom: bulk modulus) obtained for media having 1 (dashed), 2 (solid), 3 (dashed-dotted), and 4 (dotted) unit cells in the propagation direction. Regardless of the slab thickness, the extracted material parameters are virtually identical, which implies that sheets one unit cell thick are enough to characterize a bulk medium. As the wavelength inside the medium becomes comparable to the unit cell size ($\lambda_{cm}^{x} \approx 5a$), sonic crystal effects start to dominate and the effective material parameters become dependent of frequency.

the retrieved material parameters start having a significant variation with the wavelength. It is worth noting that there are three wavelengths that need to be considered. The first is the wavelength inside the background fluid, λ_{bk}, the other two are the wavelengths inside the homogenized composite medium for each direction of propagation shown in Figs. 1(b) and 1(c), λ_{cm}^{x} and λ_{cm}^{y}, respectively. We note that for our particular composite $\lambda_{cm}^{x} \approx \lambda_{cm}^{y}/2$ for large λ_{bk}'s, and, as a result, ρ_{eff}^{x} becomes significantly dependent on frequency at a larger λ_{bk}. Another consequence of this variation with wavelength is the difference between the retrieved values of the bulk modulus, which should ideally be equal, for waves propagating in the x and y directions, as depicted in Fig. 3(b). Thus, for $\lambda_{cm}^{x} \approx \lambda_{cm}^{y}/2 \approx \lambda_{bk}/2 = 5a$ (recall that a is the cell dimension), the difference between the retrieved bulk modulii is approximately 20%. We expect this discrepancy to be small enough for most applications, so that, in general, the composite can be considered homogeneous for $\min(\lambda_{bk}, \lambda_{cm}^{x}, \lambda_{cm}^{y}) > 5a$. Exceptions to this rule of thumb exist, as we will see shortly. Figure 2 shows that, as expected, for the border case of $\lambda_{cm}^{x} \approx 5a$, the pressure fields are still approximately invariant in the transverse direction.

In the above analysis, the effective material parameters were retrieved from simulations in which the composite

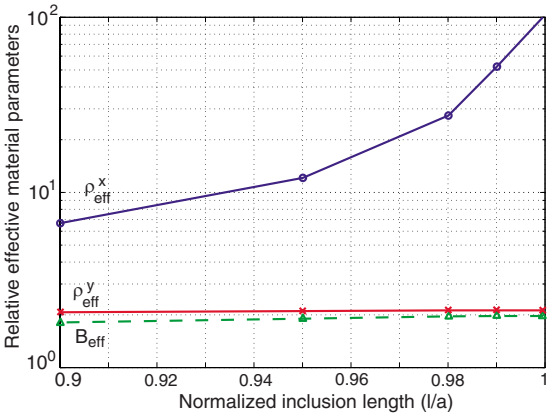

FIG. 4. (Color online) Effective material parameters versus the normalized inclusion dimension l/a. The large variation of ρ_{eff}^{x} (o) while ρ_{eff}^{y} (X) and B_{eff} ($\triangle$) remain almost unchanged demonstrate that l controls ρ_{eff}^{x} while w controls ρ_{eff}^{y}, and thus that the mass density tensor components can be controlled independently.

sample has two unit cells in the propagation direction. One may wonder whether two cells are sufficient to characterize a bulk composite. Figure 3 shows the retrieved material parameters if 1 through 4 cells are used in the simulation. As we can see, the results are virtually identical, which means that as few as one cell in the propagation direction is enough to obtain the effective material parameters of the bulk material depicted in Fig. 1(a).

Figure 3 illustrates a key characteristic of this type of cell, namely, the effective mass density anisotropy produced by the geometry of the inclusion. The physics of this phenomenon is straightforward: for one direction of propagation, the size of the inclusion fills more of the transverse dimension of the unit cell compared to the other direction, i.e., $l > w$. Consequently, the corresponding density component, ρ_{eff}^{x}, becomes greater than ρ_{eff}^{y}, because in the former case, the pressure wave propagates mostly through the more dense inclusion.

Figure 4 shows how the geometry of the inclusion controls the effective material parameters of the metamaterial. Thus, we vary l and keep $w = 0.5a$ and $\lambda_{bk} = 1000a$ (i.e., $\lambda_{bk} \rightarrow \infty$) constant. We notice the strong variation of ρ_{eff}^{x}, while the other two parameters remain almost unchanged, which demonstrates that l mainly controls ρ_{eff}^{x} and has little influence on ρ_{eff}^{y} and B_{eff}. Similarly, from considerations of symmetry, it follows that w determines the value of ρ_{eff}^{y}. The exponentional increase of ρ_{eff}^{x} with l agrees with the conclusions of Ref. 15, which predicts that ρ_{eff}^{x} is the arithmetic average between the densities of the inclusion and cell background in the limit $l = a$.

The bulk modulus matches Wood's formula[14] very well at these large wavelengths. More specifically, the effective bulk modulus is found to be the harmonic average of the bulk modulii of the cell components. As a consequence, the bulk modulus is, as expected, independent on the wave direction in the limit of low frequencies.

These observations allow us to design composite materials with effective material parameters having a large range of values. We saw previously how large values of ρ_{eff} can be

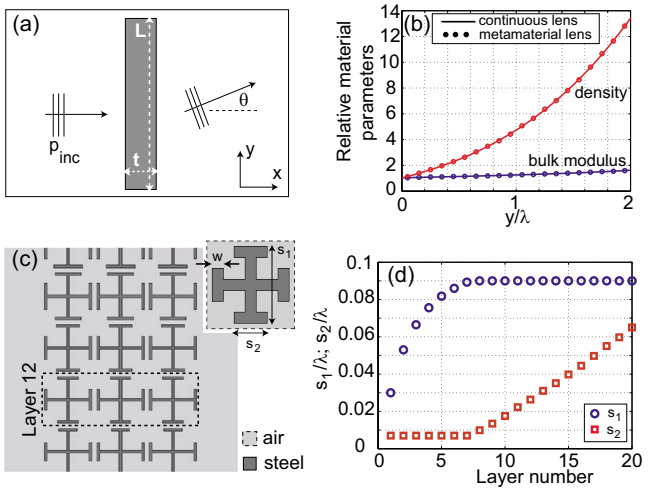

FIG. 5. (Color online) Lens design. (a) The lens changes the direction of a wave normally incident on it by an angle θ; (b) material parameters inside the theoretical lens made of a continuous, inhomogeneous material (solid curves) versus material parameters inside each one of the 20 layers of the lens realizable with acoustic composites (each dot represents the parameters inside each layer); (c) close up of the layered lens made of composite materials. The layers are numbered in ascending order from bottom to top (layer 12 is highlighted). Inset: unit cell template; (d) geometry parameters s_1 and s_2 of the unit cells used to realize each layer ($w=0.005\lambda$).

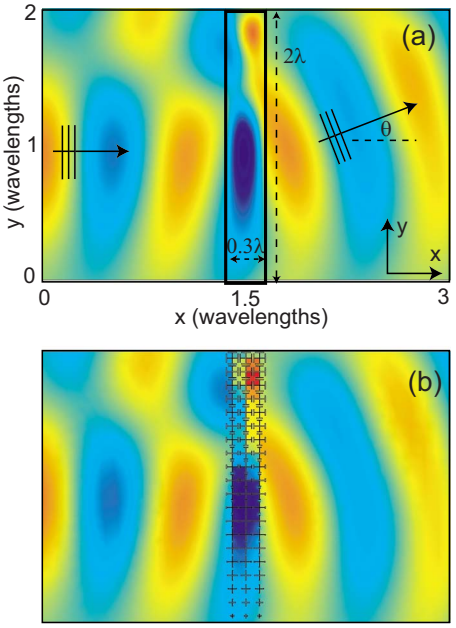

FIG. 6. (Color online) Lens performance. (a) Fields inside and around the theoretical lens. The lens bends a normally incident acoustic wave by θ degrees; (b) fields inside and around the lens realized with acoustic composites are almost identical to the fields of the theoretical lens.

obtained using high density particles. In the same way subunity values of ρ_{eff} can be achieved if the dense inclusions are replaced by materials with densities lower than that of the background fluid. For instance, if the background fluid is air, one can obtain relative density values as low as 0.2 by using inclusions made of helium. If the background fluid is water, the range of available effective bulk modulii is large, but the upper range of effective densities is much reduced because the water density is generally only an order of magnitude smaller than that of most rigid solids.

III. DESIGN OF AN ACOUSTIC BEAM-BENDING LENS

To demonstrate the efficacy of our method to devise acoustic composites, we employ it in order to design a flat, isotropic metamaterial lens of thickness $t=0.3\lambda$ and length $L=2\lambda$ capable of bending a normally incident wave propagating in air in the x direction by an angle θ [see Fig. 5(a)]. The wavelength in air is λ. Since the lens has a finite size in the transverse direction, we assume the incident wave to be a Gaussian beam whose amplitude in the plane situated 1.5λ behind the lens is given by $p_{\text{inc}}(x=0,y)=\exp[-2(y-\lambda)^2]$. We start our design by specifying the ideal material parameters we wish to obtain inside the lens.

According to diffraction theory, one way to achieve the desired lens behavior is to set the wavenumber inside the lens material, k, to have a linear variation with the transverse direction y, and to be invariant in the propagation direction x. This constraint requires the acoustic refractive index, defined as $n \equiv k/k_0 = \sqrt{\rho/B}$ (where k_0 is the wave number in air, and as before, B and ρ are relative to the parameters of air), to have the following expression:

$$n(x,y) = 1 + \frac{n_{\max} - 1}{L} y, \tag{2}$$

where $n_{\max}$ is the maximum refractive index at the $y=L$ end of the lens. Assuming a Gaussian beam normally incident on the lens, i.e., the phase is approximately constant on the first lens-air interface, $x=1.5\lambda - t/2$, the phase advance at the second lens-air interface at $x=1.5\lambda + t/2$ is

$$\phi(y) = -k_0 t\left(1 + \frac{n_{\max} - 1}{L} y\right), \tag{3}$$

which determines a bending angle of

$$\theta = \arcsin\left[\frac{t}{L}(n_{\max} - 1)\right], \tag{4}$$

Assuming $n_{\max}=2.85$, a value relatively easy to obtain with the composites described above, it follows that $\theta \approx 15°$.

One choice of material parameters, B and ρ, easier to realize using composite materials, and which result in the refractive index profile given by Eq. (2), are presented in Fig. 5(b) (see the solid curves). Similar to n, both B and ρ vary with the transverse coordinate y and are invariant with x. Figure 6(a) shows the pressure fields inside and around the theoretical lens having these material parameters, and were obtained in a numerical simulation performed with COMSOL Multiphysics. The simulation confirms the desired behavior of the lens: the normally incident Gaussian beam is deflected by approximately 15°. In order to cancel the reflections from the boundaries of the computation domain, perfectly

matched layers were placed around the domain (not shown). We also note the increased reflection of the incident beam from the upper section of the lens (i.e., around $y=L$) compared to that from the lower section around $y=0$. This effect is caused by the variation in the lens impedance η (defined as $\eta \equiv \sqrt{\rho B}$) with y: η is closer to the impedance of air at the lower end of the lens and bigger at the upper end.

Once we determined the required material parameters, we design an acoustic composite metamaterial that best approximates these parameters. First, we discretize the continuous profiles of ρ and B, or, equivalently, approximate the theoretical continuous lens medium using layers of homogeneous materials that have ρ and B specified by the dots in Fig. 5(b). We choose each layer to be 0.1λ in the transverse direction, y, and, since the desired material parameters are invariant in the x direction, each layer spans the entire lens width of $t=0.3\lambda$. Each one of these 20 resulting layers are physically implemented using acoustic composites made of unit cells that follow the template presented in the inset of Fig. 5(c). More specifically, each unit cell is a square having an edge of $a=0.1\lambda$, and contains a single steel particle whose symmetry makes the cell isotropic. By modifying the values of s_1 and s_2, we tune the material parameters of the composite generated by the unit cell. Thus, in virtue of Fig. 4, by increasing s_1 and s_2 we increase the value of ρ, while only very slightly increase the value of B. Figure 5(d) presents the values of s_1 and s_2 needed to obtain the discretized material parameters shown as dots in Fig. 5(b). The width of the segments that compose each steel particle is constant, $w=0.005\lambda$.

Figure 6(b) presents the fields generated by the Gaussian beam incident on the physical lens made of acoustic composites, while Fig. 5(c) shows a close up of the lens structure. A comparison between Figs. 6(a) and 6(b) shows that the field distribution outside, and more importantly, inside the physical lens matches very well the fields generated in the presence of the theoretical lens made of the hypothetical continuous material. The good agreement demonstrates that the composite lens made of discrete steel particles behaves almost identically to the continuous material lens, which in turn validates the composite design methodology presented here. It is worth pointing out that in the upper part of the lens the homogenization theory that allows us to attach effective material properties to the metamaterial structure holds, even though the wavelength inside the metamaterial composite becomes $\lambda_{cm} \approx 3.5a$, as demonstrated by the almost identical behavior of the theoretical lens and its metamaterial implementation.

We saw for the simple design of Sec. II that the analysis of one cell in the propagation direction was enough to characterize the bulk metamaterial. We verified this conclusion for the more complicated and realistic cell used in this section. For this purpose, we simulated a metamaterial lens that had the same structure in the transverse direction as the lens discussed above, but had only one layer in the propagation direction. A comparison between the fields in the neighborhood of this lens and the fields produced by the corresponding continuous lens shows, as before, virtually identical behavior of the two devices.

IV. CONCLUSIONS

We presented and demonstrated a design methodology for broadband, nonresonant acoustic composite metamaterials made of arrays of unit cells composed of one or more inclusions in a host fluid. By extracting the effective bulk parameters of unit cell arrays from numerical reflection and transmission simulations of a single unit cell, we showed that strong anisotropy of the effective mass density tensor can be achieved and that the effective mass density components can be independently controlled with a properly designed inclusion geometry. The effective parameters can be reliably extracted from wave reflection and transmission on a slab as thin as one unit cell, which shows that the behavior of a large slab can be determined from either simulations or measurements of a small sample. The effective bulk modulus and mass density tensor of arrays of nonresonant unit cells are nearly frequency-independent from dc to an upper frequency determined by the size of the unit cell relative to the acoustic wavelength in the metamaterial.

The entire design approach was demonstrated through the design and simulation of a flat beam-bending acoustic lens. Using efficient single unit cell simulations, we designed a series of unit cells to approximate the acoustic properties of a smoothly inhomogeneous acoustic lens. Complete simulations of the smoothly inhomogeneous lens and of the structured metamaterial approximation confirm that the wave behavior outside and even inside each lens is essentially identical. Thus, the metamaterial lens, which is straightforward to fabricate, performs just as the smoothly inhomogeneous lens. This approach can be applied to design the acoustic composite metamaterials needed to realize a wide range of devices derivable through transformation acoustics.

*bap7@ee.duke.edu
†cummer@ee.duke.edu

[1] S. A. Cummer and D. Schurig, New J. Phys. **9**, 45 (2007).
[2] H. Chen and C. T. Chan, Appl. Phys. Lett. **91**, 183518 (2007).
[3] S. A. Cummer, B. I. Popa, D. Schurig, D. R. Smith, J. B. Pendry, M. Rahm, and A. F. Starr, Phys. Rev. Lett. **100**, 024301 (2008).
[4] D. Torrent and J. Sanchez-Dehesa, New J. Phys. **10**, 063015 (2008).
[5] A. N. Norris, Proc. R. Soc. London, Ser. A **464**, 2411 (2008).
[6] R. S. Lakes, T. Lee, A. Bersie, and Y. C. Wang, Nature (London) **410**, 565 (2001).
[7] N. Fang, D. Xi, J. Xu, M. Ambati, W. Srituravanich, C. Sun, and X. Zhang, Nature Mater. **5**, 452 (2006).
[8] G. W. Milton, M. Briane, and J. R. Willis, New J. Phys. **8**, 248 (2006).
[9] S. Zhang, L. Yin, and N. Fang, Phys. Rev. Lett. **102**, 194301 (2009).
[10] Y. Cheng, F. Yang, J. Y. Xu, and X. J. Liua, Appl. Phys. Lett. **92**,

151913 (2008).
[11] J. B. Pendry and J. Li, New J. Phys. **10**, 115032 (2008).
[12] S. A. Cummer, M. Rahm, and D. Schurig, New J. Phys. **10**, 115025 (2008).
[13] D. R. Smith, D. C. Vier, T. Koschny, and C. M. Soukoulis, Phys. Rev. E **71**, 036617 (2005).
[14] A. B. Wood, *A Textbook of Sound; Being an Account of the Physics of Vibrations with Special Reference to Recent Theoretical and Technical Developments* (Macmillan, New York, 1955).
[15] M. Schoenberg and P. N. Sen, J. Acoust. Soc. Am. **73**, 61 (1983).
[16] J. R. Willis, Int. J. Solids Struct. **21**, 805 (1985).
[17] Z. Liu, X. Zhang, Y. Mao, Y. Y. Zhu, Z. Yang, C. T. Chan, and P. Sheng, Science **289**, 1734 (2000).
[18] X. Hu, K.-M. Ho, C. T. Chan, and J. Zi, Phys. Rev. B **77**, 172301 (2008).
[19] D. Schurig, J. J. Mock, B. J. Justice, S. A. Cummer, J. B. Pendry, A. F. Starr, and D. R. Smith, Science **314**, 977 (2006).
[20] A. Sihvola, *Electromagnetic Mixing Formulas and Applications* (The Institution of Electrical Engineers, London, 1999).
[21] A. M. Nicolson and G. F. Ross, IEEE Trans. Instrum. Meas. **19**, 377 (1970).
[22] V. Fokin, M. Ambati, C. Sun, and X. Zhang, Phys. Rev. B **76**, 144302 (2007).
[23] M. S. Kushwaha and B. Djafari-Rouhani, J. Appl. Phys. **84**, 4677 (1998).